UNIVERSITY OF CALIFORNIA, SAN DIEGO

Tuning 3D Collagen Fiber Topography Modulates Cancer Cell Phenotype and Migration

A thesis submitted in partial satisfaction of the requirements for the degree Master of Science

in

Bioengineering

by

Anthony Brandon Han

Committee in charge:

Professor Stephanie Fraley, Chair
Professor Karen Christman
Professor Peter Yingxiao Wang

2017

The Thesis of Anthony Brandon Han is approved and it is acceptable in quality and form for publication on microfilm and electronically:

Chair

University of California, San Diego

2017

TABLE OF CONTENTS

LIST OF FIGURES

LIST OF TABLES

LIST OF GRAPHS

ACKNOWLEDGEMENTS

I would like to thank Professor Stephanie Fraley for her guidance, inspiration, and support as the chair of my committee. Her insights proved invaluable to the success of my research experience.

I would also like to acknowledge all the members of the Fraley Lab, whose continued support expedited my research and helped me to overcome the most difficult obstacles. Our discussions helped to put even the most cryptic subjects into perspective.

This thesis, in part, is currently being prepared for submission for publication of the material. Han, Anthony; Ortiz Velez, Daniel; Fraley, Stephanie I. The thesis author was the primary investigator and author of this material.

VITA

2015	Bachelor of Science, Biomedical Engineering, University of California, Irvine
2017	Master of Science, Bioengineering, University of California, San Diego

ABSTRACT OF THE THESIS

Tuning 3D Collagen Fiber Topography Modulates Cancer Cell Phenotype and Migration

by

Anthony Brandon Han

Master of Science in Bioengineering

University of California, San Diego, 2017

Professor Stephanie Fraley, Chair

Micropatterning technologies have demonstrated that cell shape is a major regulator of cell behavior and differentiation status, but are typically limited to flat culture systems. The geometry of three-dimensional (3D) culture environments has also been shown to significantly influence cell function, including driving cancer progression and aggression. 3D tissues typically present a topographically complex fibrous adhesive environment, which is

technically challenging to replicate and modulate in a controlled manner to provide a more physiologically relevant system for studying cell behavior. In this work, we develop a technique for systematically modulating 3D collagen fiber topography and architecture using inert molecular crowding agent, polyethylene glycol (PEG). Breast cancer cells, MDA-MB-231, were then embedded into the PEG-crowded collagen hydrogels and quantitatively characterized in terms of their morphology and migration. Herein, we demonstrate that the features of collagen gels such as fiber length, fiber width, pore size, and topographical heterogeneity, can be controlled independently of bulk density and stiffness through molecular crowding during polymerization. Then, we show that these alterations result in distinct 3D matrices that embedded cells perceive and interact with. Architectural differences are found to directly influence cell morphology, migration behavior, and phenotypic heterogeneity.

CHAPTER 1: INTRODUCTION

Cancer is one of the most pressing medical challenges today, with estimates of over 1.5 million new cases and half a million deaths in the U.S. in 2016 alone [1]. The most dangerous aspect of cancer however, is a process called metastasis, which accounts for roughly 90% of all cancer-related deaths [2]. During metastasis, cancer cells from a primary tumor site break away and invade the local tissue, eventually finding a local blood or lymphatic vessel that then serves as a conduit for the metastatic cancer cells to travel to distant parts of the body. These cancer cells then exit the vessel and form a secondary tumor site in a suitable location distant from the primary tumor, often unpredictably in various tissues. Little is known about the metastatic process. It can be observed however, that the metastatic cascade is heavily reliant on cell invasiveness and migration through the local tissue and extracellular matrix (ECM) (Fig. 1). As such, cell-matrix interactions are of high interest in parsing the mechanistic drivers of tumor progression and metastasis.

One principal ECM component of interest is Type I collagen. Collagen is the most abundant protein found in solid tumors and their stromal microenvironment and provides a dense, rigid, and architecturally complex adhesive environment [3]. Particularly, in the context of breast cancer, dense breast tissues exhibiting dense mammograms (Fig. 2) are often associated with higher risks of breast cancer development and more aggressive cancers

at more advanced stages [4]. Little is known about the cause for this correlation, in part due to the highly subjective nature by which

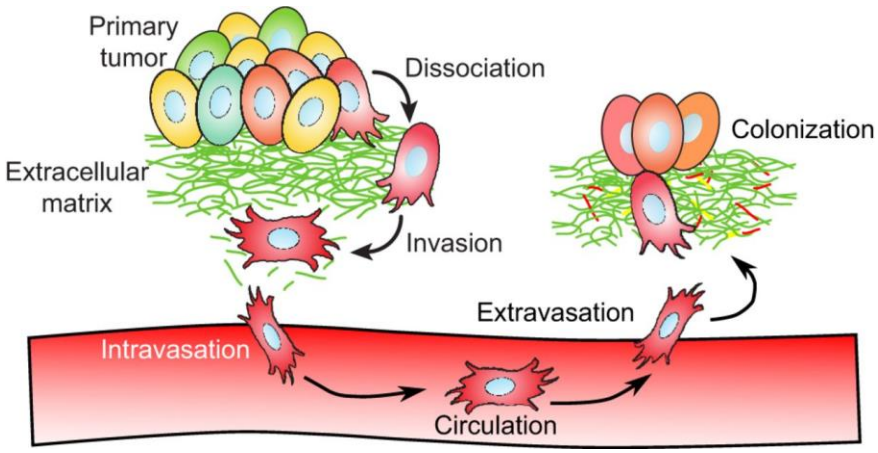

Figure 1. Overview of metastatic cascade. [5]

mammograms are currently assessed and classified. The current gold standard for analyzing mammograms is visually through a program, Cumulus, that essentially calculates the total area of breast tissue, the area of dense breast tissue, and the percentage occupied by dense breast tissue. This program however, requires a specialist to manually outline the boundaries of the breast tissue and define the dense areas [6]. This method provides some form of quantification during mammogram analysis, but does not completely remove individual subjectivity and judgement from the process. Another issue with current mammogram assessment includes the fact that a three-dimensional (3D) tissue is being visually analyzed based on its two-dimensional (2D) projection. Ultimately, the question remains as to what exactly it is about the context and environment of dense breast tissue that

drives tumor progression and aggression. It may be due to several factors such as the increased stiffness or the confinement that cells experience in these environments, or some combination of factors.

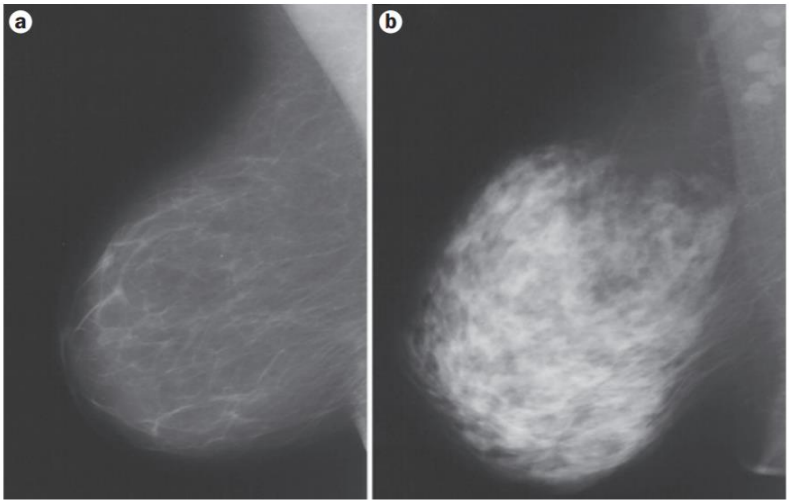

Figure 2. Mammogram comparison. Low density breast (left) vs. high density breast (right). [6]

To mechanistically study the response of cancer cell behavior to specific features of the ECM, researchers primarily rely on *in vitro* models. *In vitro* models confer unique advantages over *in vivo* models, such as the ability to execute well-defined and controlled experiments with reproducible results and higher throughput. *In vivo* conditions are highly intricate and confounded, often making it difficult to pinpoint the cause for observed phenomena. On the other hand, *in vitro* models are generally oversimplifications. Recognizing these facts and attempting to reconcile the advantages of both types of model systems, many researchers have recently moved towards studying cells in 3D *in vitro* models as opposed to on traditional 2D substrates. 3D *in vitro* models

enable researchers to study cells in a more physiologically relevant and representative context, while maintaining the flexibility and control of *in vitro* systems. It has been shown that protein function and cell behavior are distinct for cells studied in a 2D versus a 3D environment [ref all of my old papers]. Cells form intricate structures [7] or exhibit unique migration behaviors [8] in 3D systems that would not have been observed in 2D otherwise.

Despite the advantages of 3D *in vitro* model systems, several major challenges remain. One of these challenges is the difficulty in decoupling matrix parameters from one another. For example, bulk stiffness can be accomplished by increasing the ECM concentration, but often leads to higher levels of confinement, increased potential for adhesive receptor activation, and changes to the matrix architecture. Thus, it is difficult to definitively conclude whether an observed phenomenon is primarily driven by one matrix parameter or another. A number of approaches have been explored in attempts to decouple matrix parameters. To decouple stiffness from matrix density, one study utilized non-enzymatic glycation of collagen monomers prior to gel polymerization, to produce collagen hydrogels that were 3 times as stiff, without increasing the collagen concentration [9]. The limitations of this approach however, include a lengthy preliminary 5 day glycation procedure, as well as the generation of advanced glycation end products (AGE) that could influence cells that display receptors against AGE (RAGE). To decouple matrix density from matrix architecture, some studies have used macromolecular crowding (MMC). Addition of MMC during collagen polymerization was found

to produce distinct fiber topography independently of concentration. A recent study attempted this with Ficoll as the MMC agent [10]. However, cells were seeded on top of the hydrogel. Not only does seeding cells on top versus embedding within a hydrogel present significantly different environments and cues to the cells, but the decision to seed cells on top potentially minimizes contact between the cells and the crowding agent. This led to questions about the potential negative impact that Ficoll may have on cell viability and behavior. Indeed other studies have shown that Ficoll is cytotoxic [11].

With these limitations in mind and a need for a reliable and tunable 3D *in vitro* model, we propose a novel hybrid system that employs inert synthetic polyethylene glycol (PEG) molecules as MMC agents to modulate fiber topography and gel architecture of a naturally derived collagen matrix. Furthermore, this can be accomplished independently of collagen concentration, while embedding cells inside of the hydrogels. The premise for the mechanism of action of our MMC-inspired system (Fig. 3) is that PEG molecules occupy a fraction of the interstitial space in between collagen monomers, ultimately increasing the number of collagen fiber nucleation sites. As a result, the total number of fibers that are produced also increases. Since the amount of collagen being used is unchanged, the same amount of collagen monomers now have a greater number of nucleation sites to associate with, thus making each of the final fibers shorter and thinner than those formed in the absence of the MMC agent.

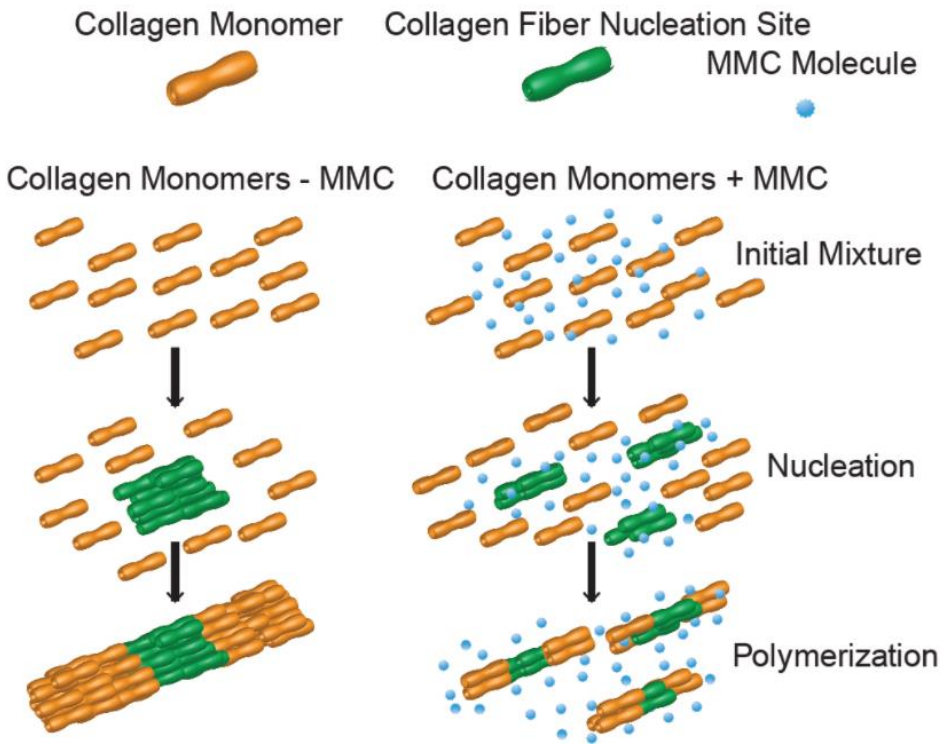

Figure 3. Overview of MMC mechanism of action.

In this work, we first test whether PEG can be used as an MMC agent to create distinct matrices by reliably tuning the fiber topography and architecture of a 3D collagen gel, independently of bulk collagen concentration. Second, we compare our MMC agent of choice, PEG, to the MMC agent used by the other study, Ficoll, and found that Ficoll had a negative impact on cells, while PEG did not. Third, we show that MDA-MB-231 breast cancer cells embedded into these various matrices exhibited different morphology, motility, and phenotype. Lastly, we draw correlations between the responses of the matrix to the varying levels of MMC crowding and that of the cells to the distinct matrices that they are embedded in, to provide insight into

cell-matrix interactions and attribute specific matrix characteristics to potentially responsible modulators of cell behavior.

CHAPTER 2: MATERIALS AND METHODS

2.1. Cancer cell culture

MDA-MB-231 (MDA) breast cancer cells were ordered from ATCC (Manassas, VA) and cultured in Dulbecco's Modified Eagle's Medium (Life Technologies, Carlsbad, CA) supplemented with fetal bovine serum (Corning, Corning, NY) and gentamicin (Life Technologies, Carlsbad, CA), at 37 °C and 5% CO_2. Culture media was changed every other day as needed. Cells were cultured to confluence prior to being trypsinized and embedded inside of collagen gels. Embedded MDAs were cultured for a week to observe long-term phenotypic differences.

2.2. Collagen gel preparation

2.2.1. Collagen gels polymerized in the presence of MMC molecules

High concentration, rat tail acid extracted type I collagen was ordered form Corning (Corning, NY). MMC agents, PEG 8000 and Ficoll 400, were ordered in powder form from Sigma-Aldrich (St. Louis, MO) and reconstituted in PBS (Life Technologies, Carlsbad, CA) prior to usage. Trypsinized cells to be embedded, were first mixed with 1x reconstitution buffer composed of sodium bicarbonate, HEPES free acid, and nanopure water. Appropriate amounts of MMC agent, PEG or Ficoll, were then added to produce final concentrations of 0, 2, 4, 6, 8, and 10 mg ml^{-1} PEG [denoted by P0, P2, P4, P6, P8, P10] or 25 mg ml^{-1} Ficoll [denoted by F25]. Afterwards, collagen solution was then added to the mixture for a final concentration of 2.5 mg ml^{-1} collagen. Finally, pH of the final mixture was adjusted using 1N sodium

hydroxide, prior to polymerization via incubation at 37 °C (~20-30 minutes). Gels were prepared inside of 48-well plates with a total volume of 200μl. Following gel polymerization and solidification, MMC molecules were washed out of the collagen gels by rinsing with PBS 3x for 5 min each. Cell culture media was then added on top of the gels after and changed every two days as necessary.

2.2.2. MMC control experiments

To ensure that the MMC molecules being used were truly inert, we investigated any potential effect that the MMC molecules may have on cells independent of the changing matrix architecture. We conducted a series of MMC control experiments, where MDAs were embedded inside of three 2.5 mg ml^{-1} collagen gels. After the gels had polymerized, normal culture media was added on top to one of the gel, while the other two either had 10 mg ml^{-1} PEG or 25 mg ml^{-1} Ficoll added into the media on top. The MMC molecules were left in the media and allowed to diffuse down into the gel with the cells. Subsequent media changes would also include appropriate amounts of MMC agent to maintain the PEG and Ficoll concentrations in the gel.

2.3. Imaging

2.3.1. Confocal reflection imaging of collagen architecture

Collagen matrix architecture and topography was investigated by imaging gels using confocal reflection microscopy (CRM) with a Leica SP5 inverted confocal microscope. Collagen fibers were imaged by exciting with and collecting backscattered light at 488nm.

2.3.2 Time lapse imaging of cells

Time lapse microscopy was conducted using a Nikon Ti-E inverted microscope to analyze cell motility and migration behavior, morphology, and proliferation and viability. Cells were allowed to settle in the collagen gel in the incubator for approximately 7 h after gel polymerization; time-lapse imaging began at around the 8^{th} hour after the cells were embedded into the collagen gels. Each gel was imaged over 6 fields of view (FOV) for a period of 15 h, with images being taken every 2 min.

2.3.3 Cell proliferation assay

Cell viability was assessed using a Live and Dead Cell Assay (Abcam, Cambridge, UK). Intact, viable cells fluoresce green (imaged under FITC channel) while dead cells fluoresce red (imaged under TRITC channel). The average number of live cells, dead cells, and live cell viability percentages were calculated over 4 FOVs per condition. Live cell viability % is defined as the number of live cells / the total number of cells * 100.

2.4 Data analysis

2.4.1. Matrix analysis

All matrix analyses were done using the CRM images of the collagen gels in each condition over 3 FOVs. Fiber analysis was conducted in CT-FIRE (LOCI, University of Wisconsin, WI) (Fig. 4) by measuring individual fiber length and width. Pore size was calculated by thresholding in NIS-Elements. Homo-/heterogeneity of the matrices were characterized by calculating the

coefficient of variation (CV) of fiber length, fiber width, and pore size. Stiffness measurements were taken using a cone and plate rheometer.

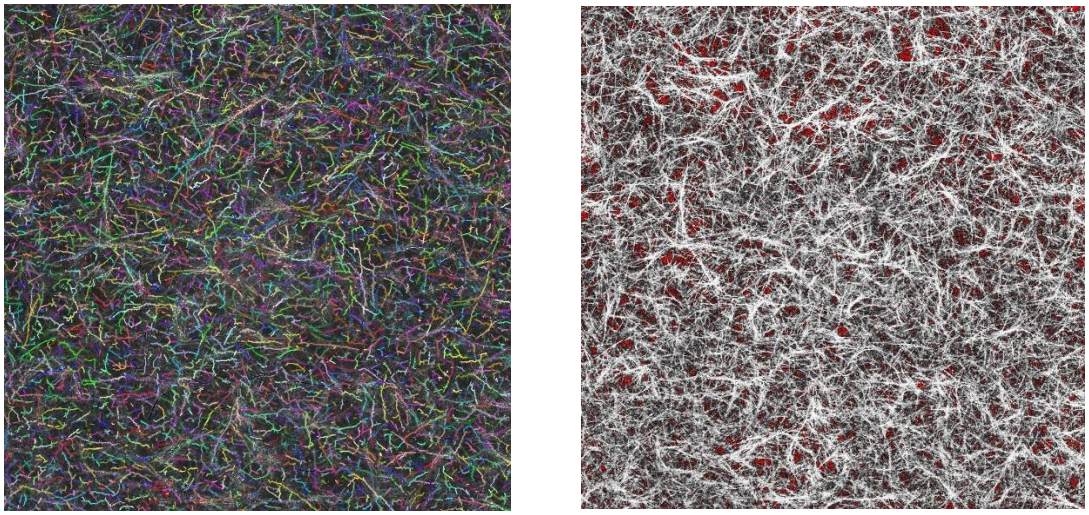

Figure 4. Representative matrix analysis images. Fiber analysis in CT-FIRE (left) and pore size analysis in NIS-Elements (right).

2.4.2. Cell analysis

Individual cells in the time lapse videos were tracked in Metamorph (Fig. 5) for motility characterization. Within the 15 h time lapse window, cells were analyzed in terms of the total path length traveled, their average speed, the invasion distance (displacement), and the persistence of their migration (defined as the invasion distance / the total path length traveled). Cell morphology analysis was conducted using images of the cells during the 15th hour after implantation into the gel, in terms of circularity (computed as an index through NIS-Elements by the equation: { [4*π*area] / perimeter^2}) and

aspect ratio (defined as the length of the major axis / minor axis).

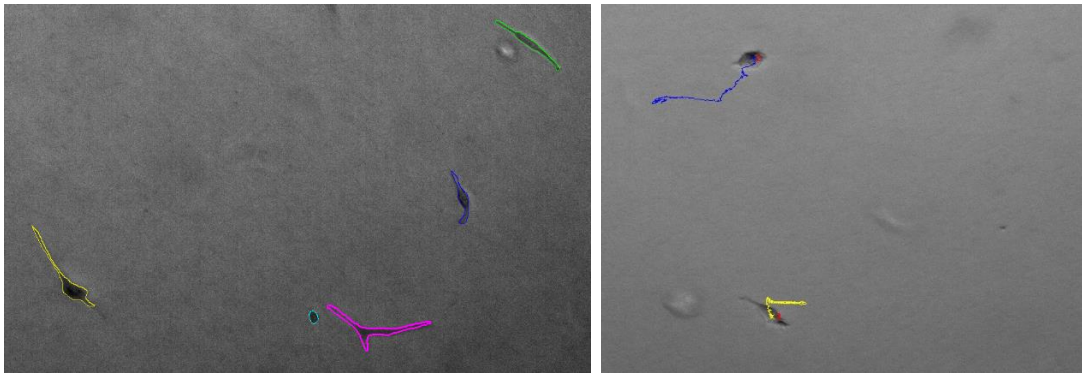

Figure 5. Representative cell analysis images. Cell morphology analysis in NIS-Elements (left) and single cell tracking in Metamorph (right).

2.4.3. Correlation analysis

Correlations were calculated in terms of the Spearman correlation coefficient. Correlations were drawn between various matrix parameters to evaluate whether they had been decoupled, as well as between matrix and cell parameters to investigate cell-matrix interactions.

2.4.4. Statistics

Data was statistically analyzed using one-way analysis of variance (ANOVA) and Tukey's post hoc test in GraphPad Prism (v5). N=3 independent biological replicates for each condition tested. Statistical significance was reported for values of $p < 0.05$ and denoted with asterisks as $p<0.001$, ***; $p<0.01$, **; $p<0.05$, *.

CHAPTER 3: RESULTS

3.1. MMC creates distinct 3D matrices

3.1.1. Matrix architecture and fiber topography

The introduction of MMC PEG molecules into the collagen monomer solution prior to gel polymerization, creates distinct matrix architectures with not changes to the bulk collagen concentration. These differences could clearly be seen visualized in the reflection micrographs (Fig. 6). Quantitative characterization of the

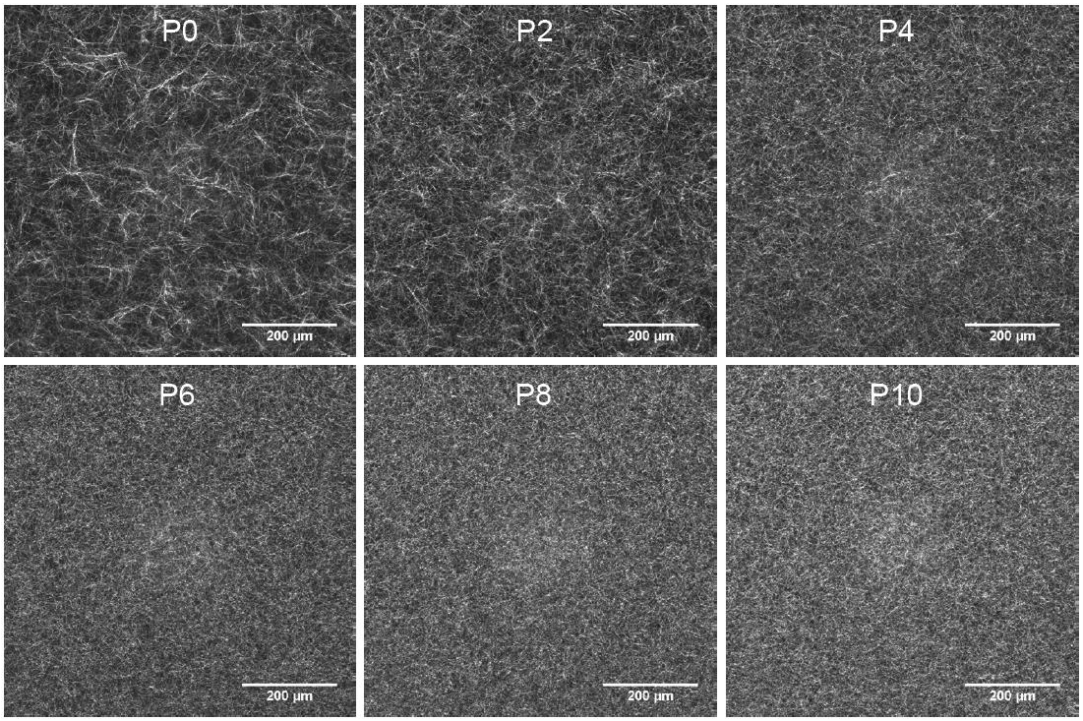

Figure 6. Representative CRM images of collagen matrix. Conditions: P0 (2.5 mg ml^{-1} collagen); P2-P10 (2.5 mg ml^{-1} collagen + 2-10 mg ml^{-1} PEG).

fiber topography, revealed that the introduction of MMC molecules resulted in collagen gels with shorter and thinner fibers (Graphs 1-3). This result is

consistent with the notion that the introduction of MMC induces more collagen fiber nucleation sites to occur, thus giving collagen monomers more sites to associate with and ultimately form more fibers with less monomers per fiber. The CV was calculated for fiber length, fiber width, and pore size to assess heterogeneity in these parameters as a function of crowding (Graphs 4-6).

Graph 1. Characterization of mean fiber length as a function of the extent of crowding. Increasing the levels of MMC creates matrices with shorter fibers. N=3 biological replicates for each condition. Statistical significance tested by ANOVA and reported as p<0.001, ***; p<0.01, **; p<0.05, *.

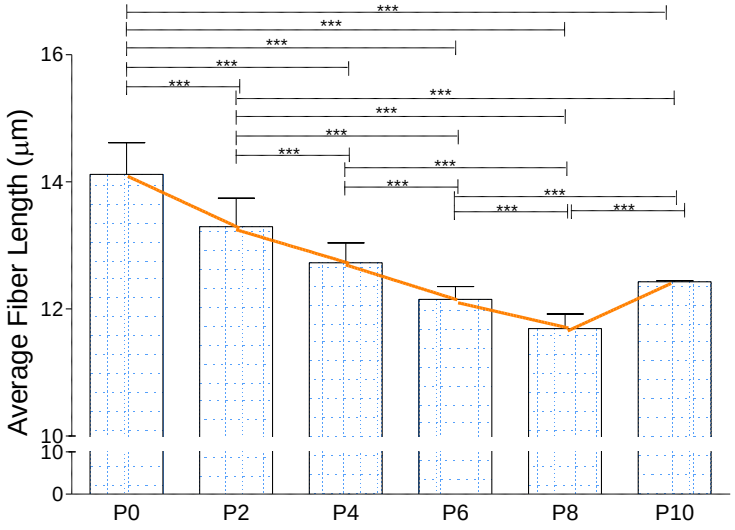

Graph 2. Characterization of mean fiber width as a function of the extent of crowding. Increasing the levels of MMC creates matrices with thinner fibers. N=3 biological replicates for each condition. Statistical significance tested by ANOVA and reported as p<0.001, ***; p<0.01, **; p<0.05, *.

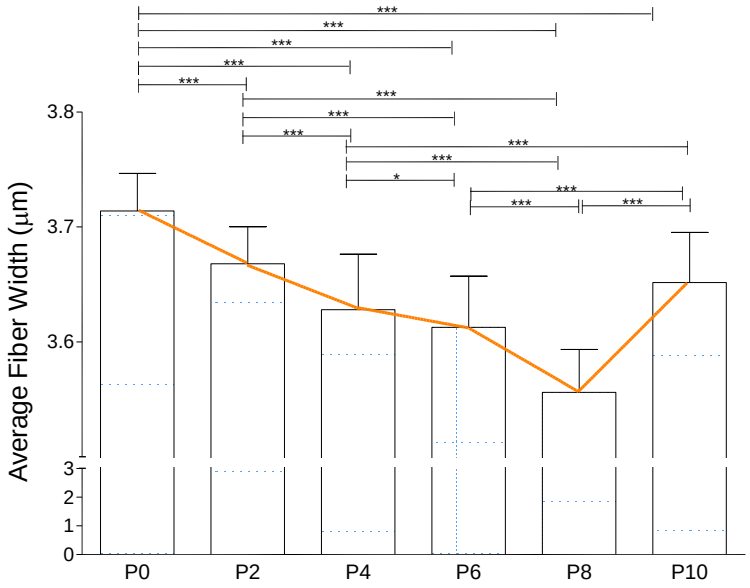

Graph 3. Characterization of mean pore size as a function of the extent of crowding. Increasing the levels of MMC creates matrices with smaller pores. N=3 biological replicates for each condition. Statistical significance tested by ANOVA and reported as p<0.001, ***; p<0.01, **; p<0.05, *.

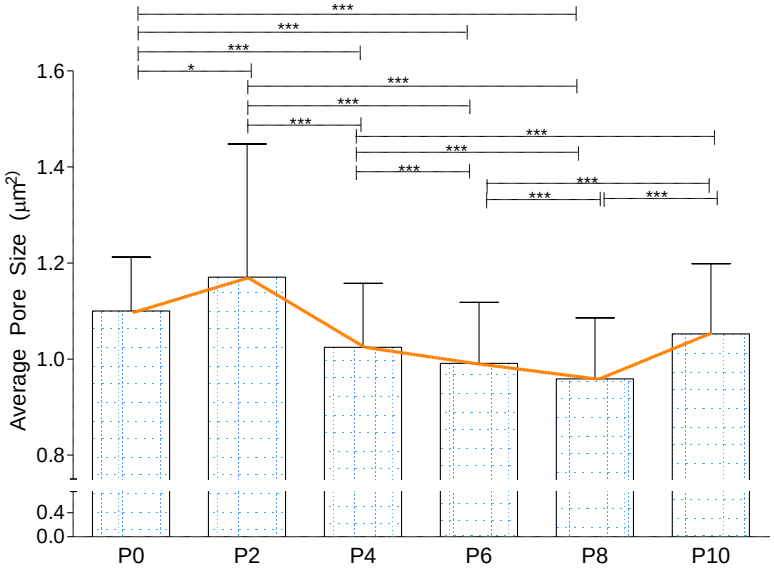

A general decrease in CV was observed in all three cases as the level of MMC increased. This demonstrated that the matrix architecture became more homogeneous from the introduction of MMC.

Graph 4. Heterogeneity of fiber length as a function of the extent of crowding. Increasing the levels of MMC creates matrices with fibers of more equivalent length. N=3 biological replicates.

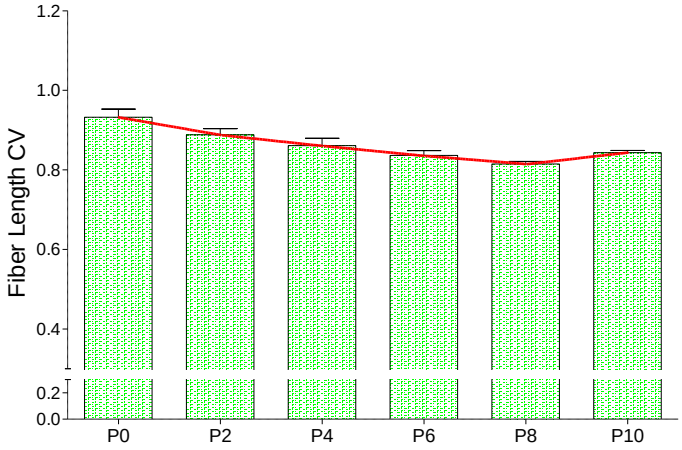

Graph 5. Heterogeneity of fiber width as a function of the extent of crowding. Increasing the levels of MMC creates matrices with fibers of more equivalent width. N=3 biological replicates.

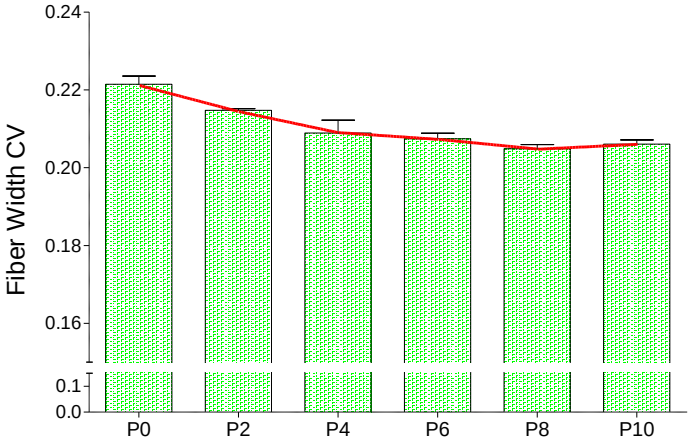

Graph 6. Heterogeneity of pore size as a function of the extent of crowding. Increasing the levels of MMC creates matrices with pores of more equivalent size. N=3 biological replicates.

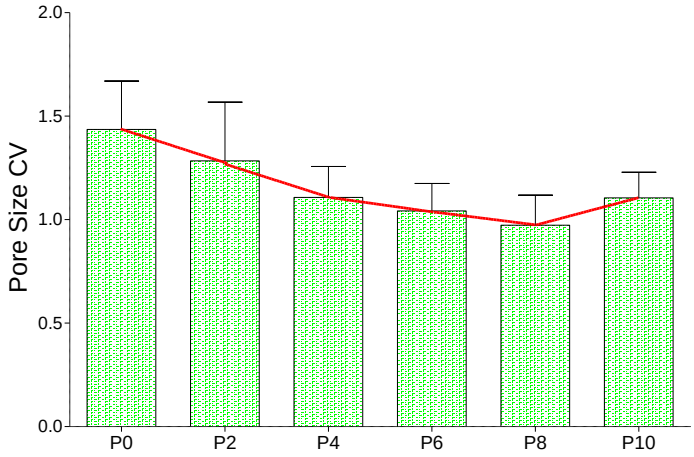

3.1.2. Bulk matrix stiffness

Having induced distinct matrix architectures through various levels of MMC, we then probed the overall bulk stiffness of the gels to determine whether architecture was decoupled from stiffness when the bulk concentration of collagen was held constant. No statistically significant differences in bulk gel stiffness were observed, as measured by shear rheometry (Graph 7), when comparing the most extreme cases (P0 vs. P10). This indicated that the changes in the architectures induced through increased levels of MMC, did not influence the overall stiffness of the gel. Thus our MMC technique decoupled matrix stiffness from fiber topography.

Graph 7. Elastic modulus of control and maximally crowded matrix. No statistical significance was found in the differences in storage modulus of the pure collagen gel and that of the maximally crowded gel (10mg ml^{-1} PEG). N=3 biological replicates. Statistical significance tested by ANOVA and reported as p<0.001, ***; p<0.01, **; p<0.05, *.

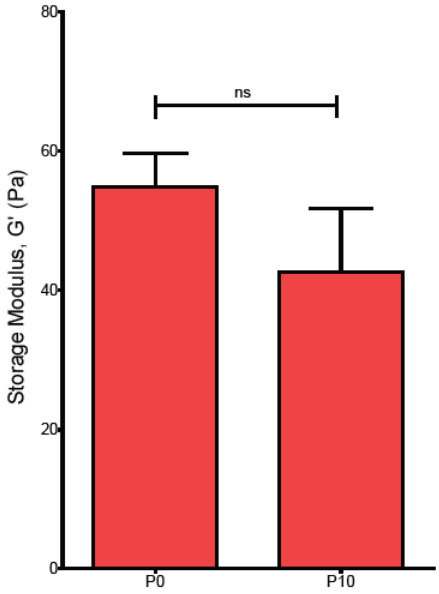

3.1.3. Fiber parameters and porosity are correlated

The ECM is a network characterized by numerous interdependent matrix parameters, so it is extremely difficult to decouple all parameters from one another. While the bulk gel stiffness as well as collagen concentration have been decoupled from the changes in the matrix architecture due to MMC, the fiber parameters and pore size were still correlated (Graphs 8-10). This indicates that MMC enables the matrix architecture to be modulated independently of concentration and stiffness, but cannot decouple matrix parameters characterizing the architecture and fiber topography from each other.

Graph 8. Correlation of fiber length with fiber width. As fiber length increases, fiber width also generally increases. Correlation strength measured by Spearman correlation coefficient.

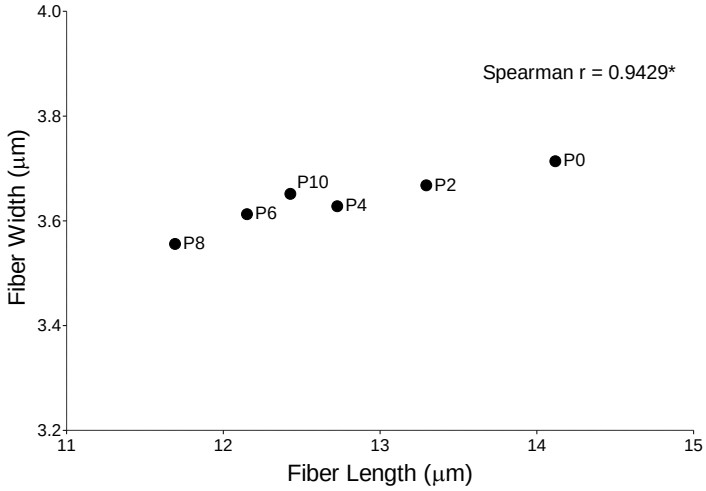

Graph 9. Correlation of fiber length with pore size. As fiber length increases, pore size also generally increases. Correlation strength measured by Spearman correlation coefficient.

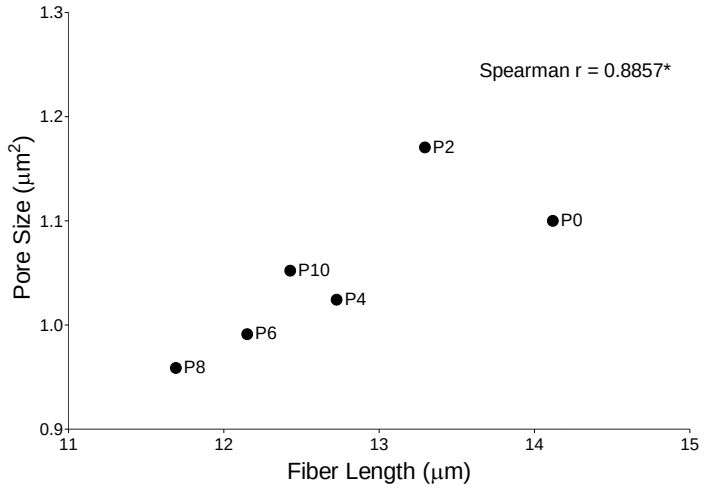

Graph 10. Correlation of fiber width with pore size. As fiber width increases, pore size also generally increases. Correlation strength measured by Spearman correlation coefficient.

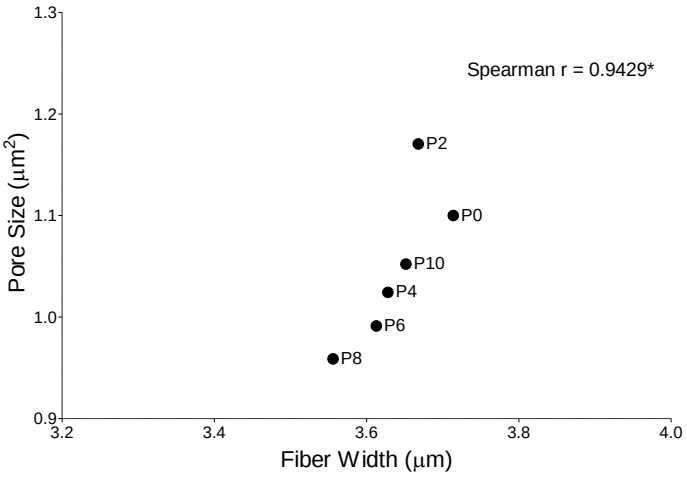

3.2. MMC effect on cells

Having observed changes in the matrix architecture due to different MMC levels, we then sought to investigate how cells behaved differently in these distinct matrices. However, we needed to first ensure that our MMC molecules were truly inert, and that they would not impact cells except through modulation of the matrix. This is critical for us to be able to attribute any observed variations in cell morphology, motility, and phenotype solely to changes in the matrix architecture and topography. MDAs were embedded into 3 separate 2.5 mg ml^{-1} collagen gels that were polymerized in the absence of MMC agents. Then normal culture media was added on top of the control, while the maximal amount of MMC agent was added to the other two in the media and allowed to diffuse through the gel: 10 mg ml^{-1} PEG (P10) and 25 mg ml^{-1} Ficoll (F25).

3.2.1 Cell viability in presence of MMC agent

We first examined the potential impact of MMC on cell viability and proliferation rates. After a week in culture, Live and Dead Assay staining (Fig. 7) showed that the total number of cells in the Ficoll condition were considerably lower, while the ratio of dead to live cells was much higher. Averages over four FOVs in each replicate demonstrated that Ficoll negatively impacted both cell proliferation rates as well as live cell viability, while PEG did

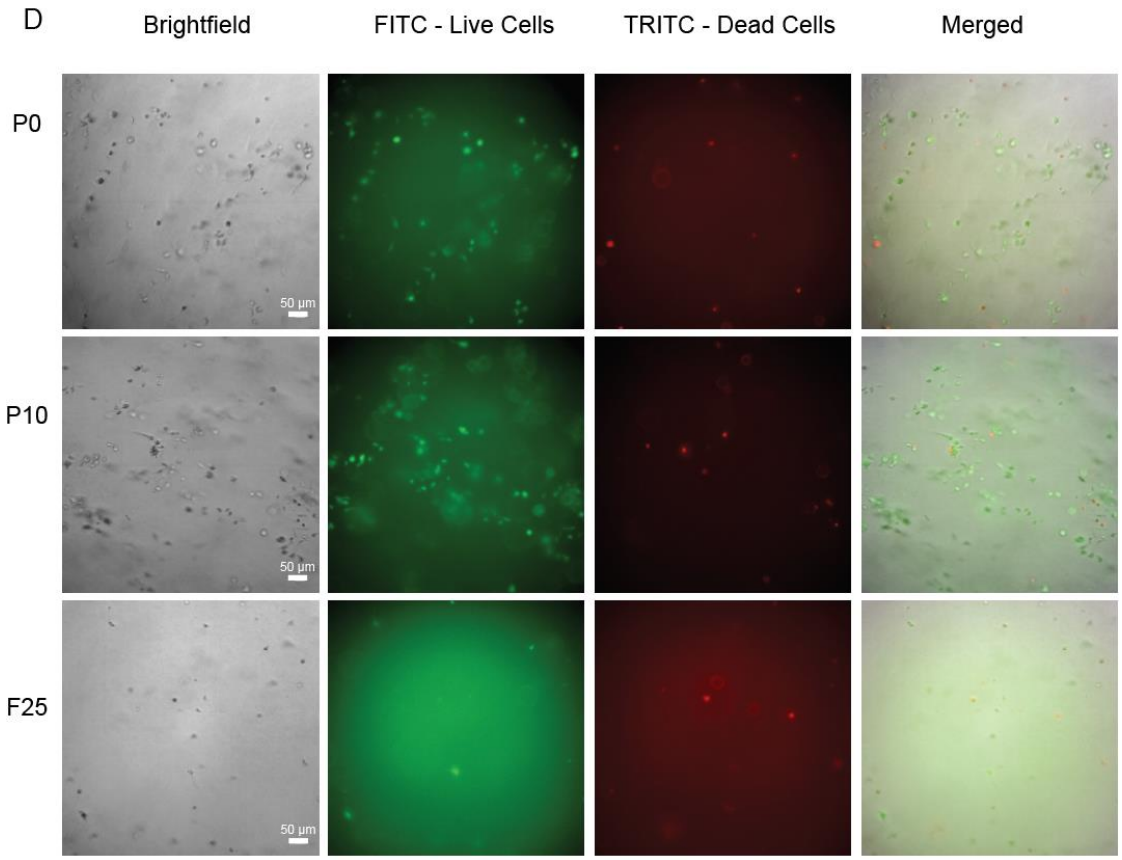

Figure 7. Live and Dead Assay staining of cells in collagen gels in the presence of MMC molecules.

not have any significant influences (Graph 11, 12). From these results, we decided to exclude Ficoll as an MMC agent and only use PEG moving forward.

Graph 11. Ficoll negatively impacts cell proliferation. The total number of cells in the Ficoll condition was drastically lower while the ratio of dead:live cells was higher.

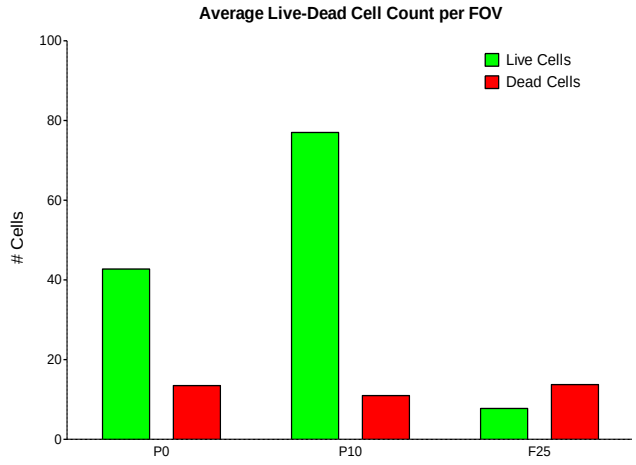

Graph 12. Ficoll negatively impacts live cell viablity. Live cell viability was less than 50% and much lower in the Ficoll condition compared to that in the control and PEG condition. No statistical significance was found in the viability differences between the control and the PEG condition. N=3 biological replicates for each condition. Statistical significance tested by ANOVA and reported as p<0.001, ***; p<0.01, **; p<0.05, *.

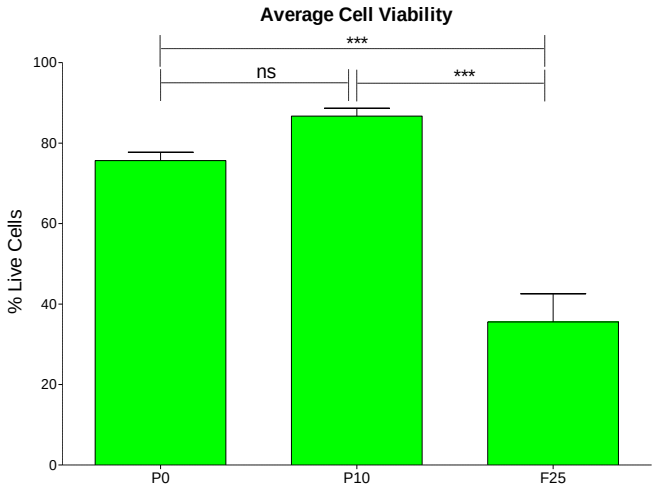

3.2.2 Cell shape in the presence of MMC agent

In order to truly establish PEG as an inert MMC agent, we then proceeded to analyze the morphology of cells in the presence of PEG. We found that PEG, by itself, has no effect on cells in terms of their morphology either (Graph 13).

Graph 13. PEG has no effect on cell morphology. No statistical significance was found in the circularity differences between the control and the PEG condition. N=3 biological replicates for each condition. Statistical significance tested by ANOVA and reported as p<0.001, ***; p<0.01, **; p<0.05, *.

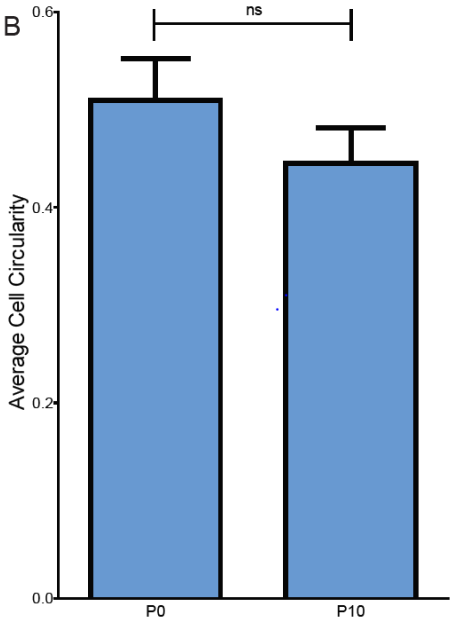

3.2.3 Cell motility in presence of MMC agent

Finally, we also analyzed the motility of cells in the presence of PEG. Again, we found that PEG, by itself, does not influence cell motility (Graph 14). From these results, we concluded that PEG was indeed an inert MMC molecule that would not affect cell proliferation, viability, morphology, nor

motility, solely due to its presence in the collagen matrix while the gel is polymerizing.

Graph 14. PEG has no effect on cell motility. No statistical significance was found in the differences in the distance traveled between the control and the PEG condition. N=3 biological replicates for each condition. Statistical significance tested by ANOVA and reported as p<0.001, ***; p<0.01, **; p<0.05, *.

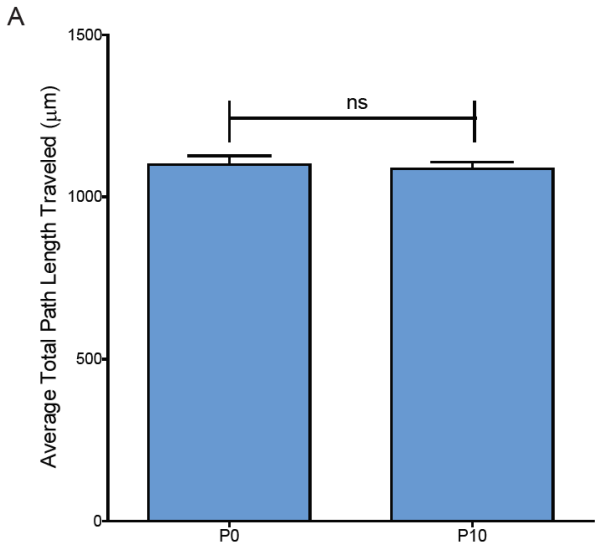

3.3. Cells behave differently in distinct matrix architectures

Having established that PEG is an inert molecule, we then proceeded with introducing MMC into the collagen gel polymerization process while simultaneously embedding cells.

3.2.1 Cell morphology in distinct matrix architectures

We first examined the influences of the matrix architecture on cell morphology. We observed that cells in MMC altered matrices, were significantly rounder and less elongated than cells in the control condition. This could be seen visually from the bright field images taken of the cells at the 15th

hour mark after embedding (Fig. 8). Quantifying cell circularity and aspect ratio, we found that cells in any matrix altered by any amount of PEG, were significantly different from the control, and demonstrated greater circularity and lower aspect ratios (Graphs 15, 16).

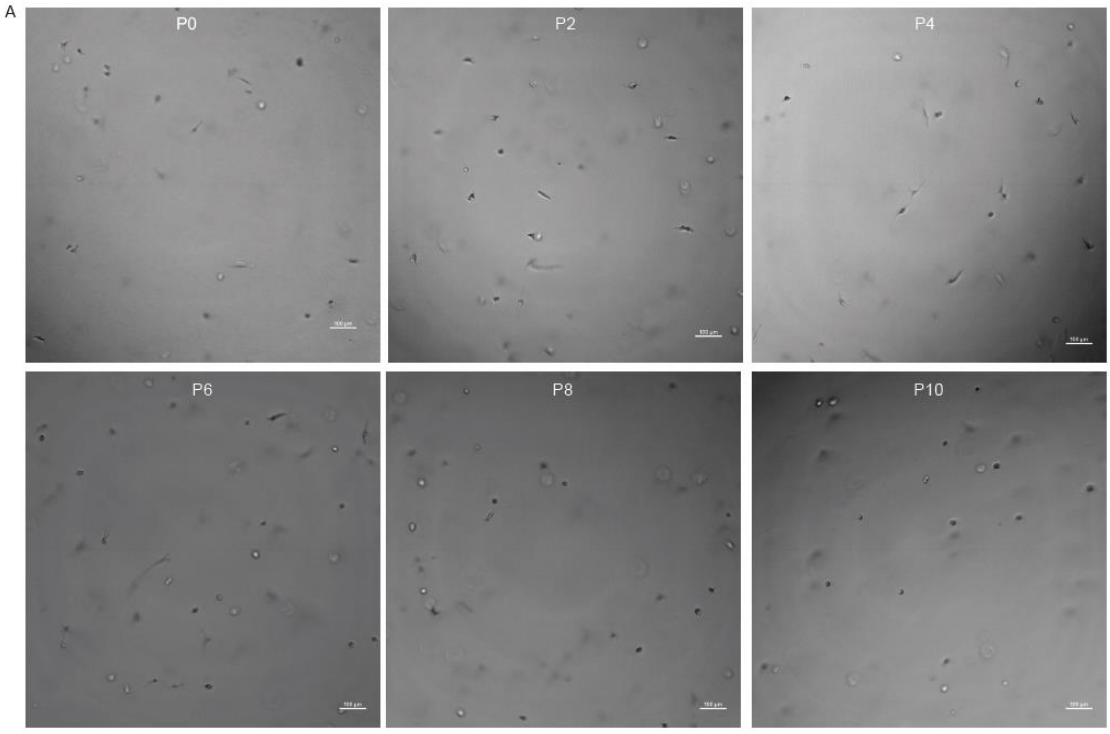

Figure 8. Live and Dead Assay staining of cells in collagen gels in the presence of MMC molecules.

Graph 15. Cells in matrices altered by MMC are more circular. N=3 biological replicates for each condition. Statistical significance tested by ANOVA and reported as p<0.001, ***; p<0.01, **; p<0.05, *.

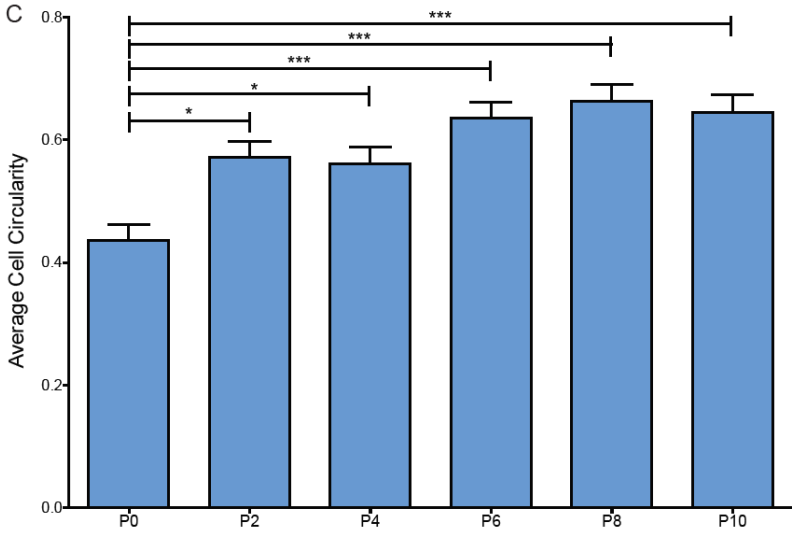

Graph 16. Cells in matrices altered by MMC are less elongated. N=3 biological replicates for each condition. Statistical significance tested by ANOVA and reported as p<0.001, ***; p<0.01, **; p<0.05, *.

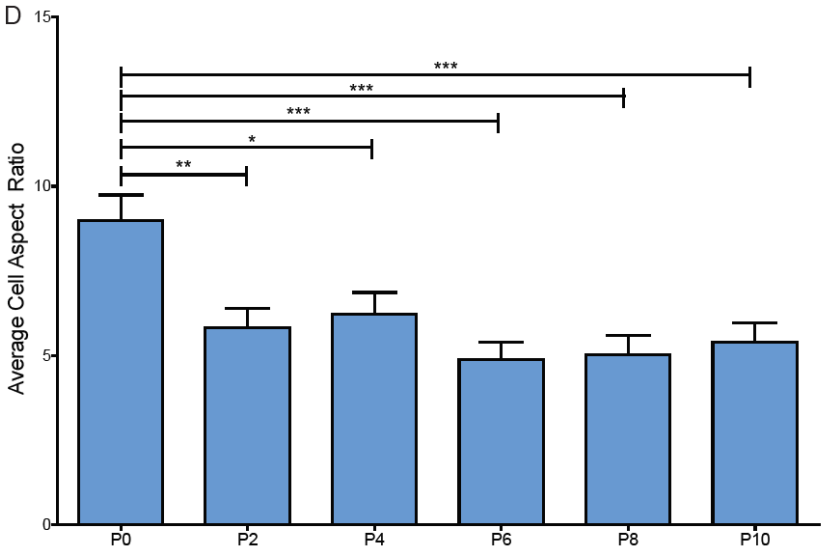

3.2.1 Cell motility in distinct matrix architectures

Next, we looked at how cell motility changes in various matrices. We found that cells generally moved slower and traveled a shorter distance when embedded in gels altered by MMC, compared to those in the control (Graphs 17, 18). Cells also appear to exhibit smaller invasion distances and move more randomly with lower persistence (Graphs 19, 20).

Graph 17. Cells in matrices altered by MMC move slower. N=3 biological replicates for each condition. Statistical significance tested by ANOVA and reported as p<0.001, ***; p<0.01, **; p<0.05, *.

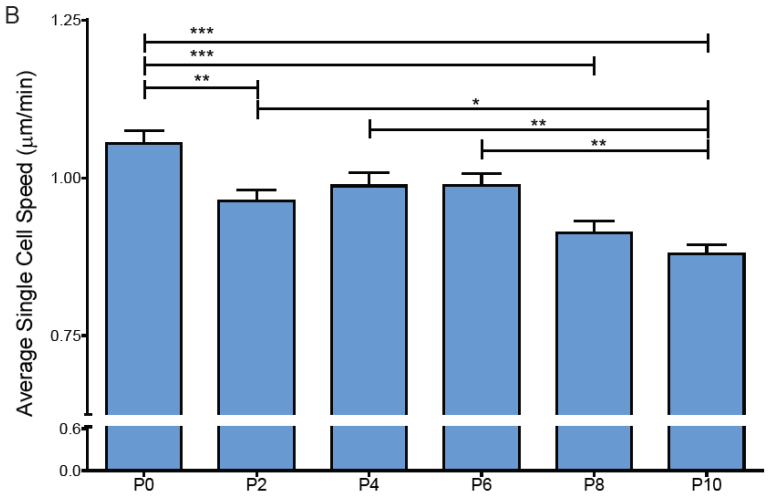

Graph 18. Cells in matrices altered by MMC travel over a shorter distance. N=3 biological replicates for each condition. Statistical significance tested by ANOVA and reported as p<0.001, ***; p<0.01, **; p<0.05, *.

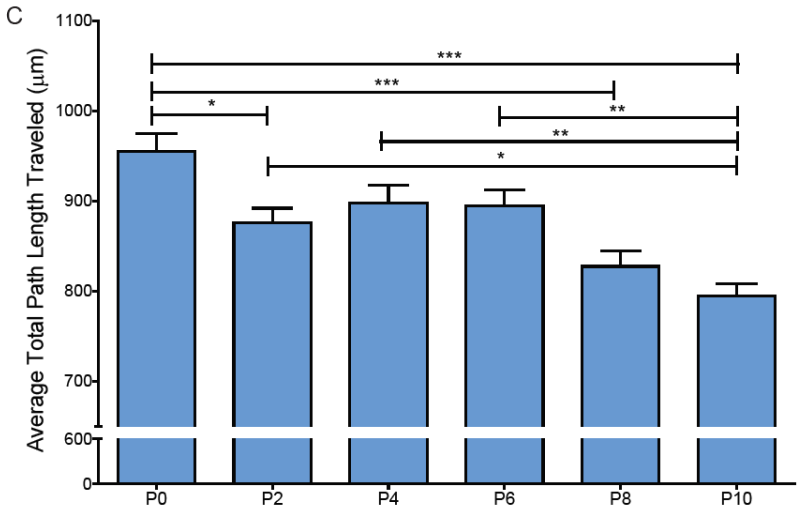

Graph 19. Cells in matrices altered by MMC travel closer to their initial starting location. N=3 biological replicates for each condition. Statistical significance tested by ANOVA and reported as p<0.001, ***; p<0.01, **; p<0.05, *.

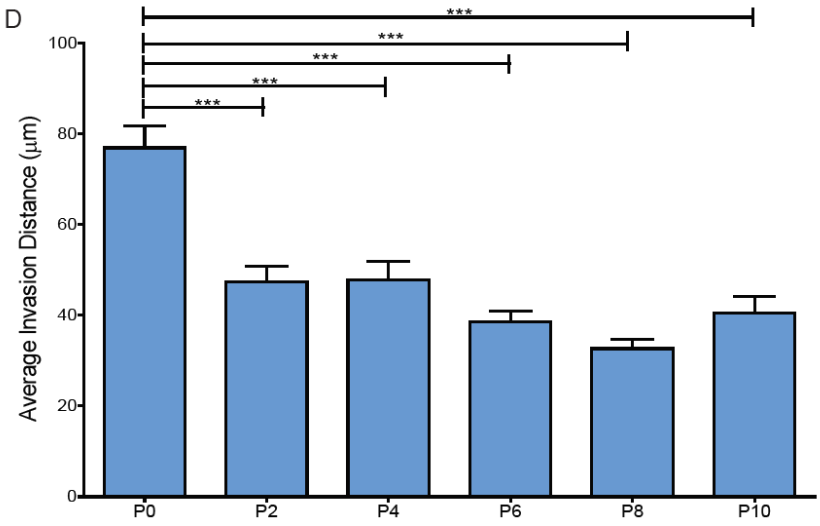

Graph 20. Cells in matrices altered by MMC travel more randomly, in a less persistent manner. N=3 biological replicates for each condition. Statistical significance tested by ANOVA and reported as p<0.001, ***; p<0.01, **; p<0.05, *.

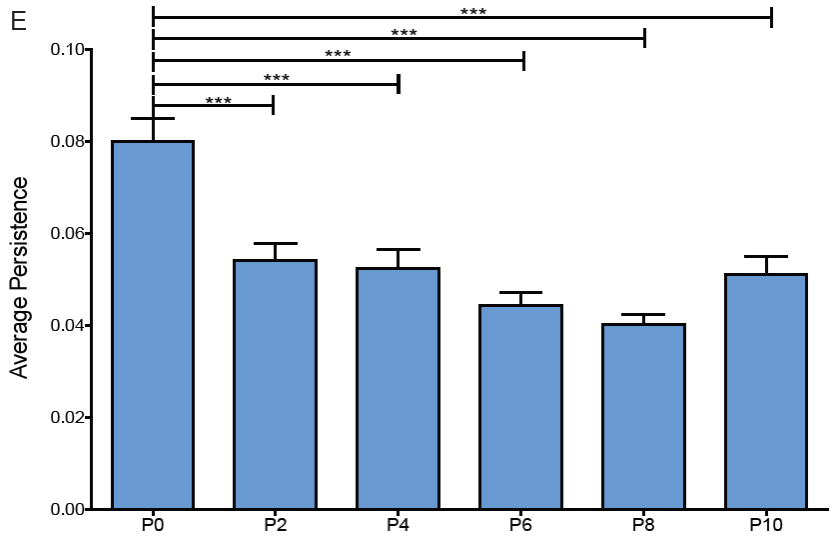

3.2.1 Week-long cell phenotype in distinct matrix architectures

Additionally, we left MDAs in culture in the various matrices for a week to evaluate their phenotype over a longer period. Interestingly, we observed that just by changing the matrix architecture, cells expressed different phenotypes (Fig. 9). Cells in the control and less MMC crowded conditions (P0-P4) were primarily located separately from one another as single cells. Cells in the higher MMC crowded conditions (P6-P10) however, organized themselves to form coherent, interconnected structures. This collective phenotype begins to appear in the P6 condition (transition point) and is even more pronounced in P8 and P10.

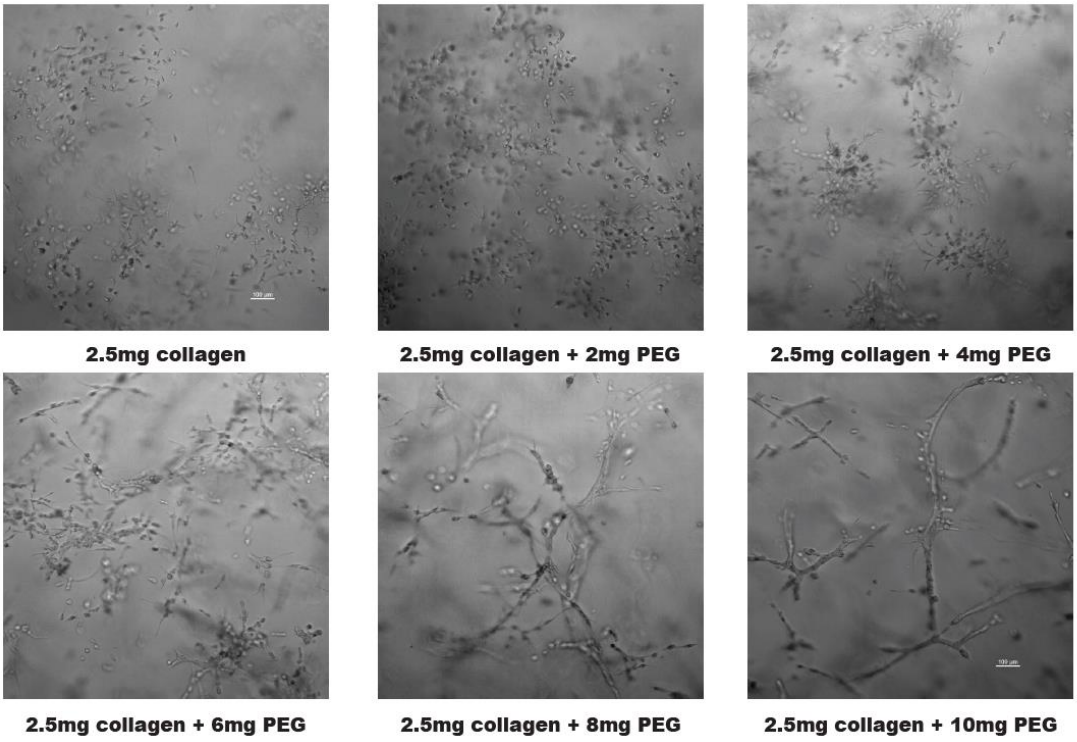

Figure 9. Representative bright field micrographs of week-long phenotypes. Cells in more crowded matrices (P6-P10) organize into coherent, interconnected structures. While cells in less crowded matrices (P0 P4) appear to remain individually associated.

3.6. Cell-matrix interactions

Having observed significant changes to both the matrix architecture as well as differences in cell morphology, motility, and phenotype when embedded into these distinct matrices, we sought to better understand the architectural feature(s) that drive cell behavior. To do so, we assessed how matrix parameters predicted cell behavior through correlation analysis. Additionally, we attempted to deduce whether specific matrix parameters were responsible for inducing the collective phenotype.

3.6.1 Cell morphology modulation by matrix architecture

Comparing changes in matrix architecture to changes in cell shape, we found that the cell shape was only significantly correlated with the fiber length, and not fiber width or pore size. Fiber length was negatively correlated with cell circularity while positively correlated with cell aspect ratio (Table 1). This suggests that fibers become shorter as the MMC crowding levels increased, and cells embedded in these matrices became more circular and less elongated.

Table 1. Strength and significance of cell shape modulation by fiber topography. Correlation strength indicated by Spearman's correlation coefficient. N=3 biological replicates for each condition. Statistical significance reported as p<0.001, ***; p<0.01, **; p<0.05, *.

	Cell circularity (mean)	Cell aspect ratio (mean)
Fiber length (mean)	-0.8857*	0.8857*
Fiber width (mean)	n.s.	n.s.
Pore size (mean)	n.s.	n.s.

3.6.2 Cell motility modulation by fiber architecture

Furthermore, we compared changes in the matrix architecture to the changes in cell motility and found that fiber length, fiber width, and pore size were all significantly and positively correlated with the invasion distance and persistence of embedded cells. On the other hand, the total path length traveled and the speed that individual cells moved at were not significantly correlated with any of matrix parameters. These relationships suggest that cells embedded in more crowded matrices invaded less and moved less persistently, but moved at roughly the same speed and traveled similar total

path lengths independently of the environment they were in (Table 2). As such, path length and single cell speed may only depend on intrinsic factors inherent to the cell, while invasion distance and persistence may depend on extrinsic factors that are dictated by the environment and the matrix that cells are in.

Table 2. Strength and significance of cell migration modulation by fiber topography. Correlation strength indicated by Spearman's correlation coefficient. N=3 biological replicates for each condition. Statistical significance reported as p<0.001, ***; p<0.01, **; p<0.05, *.

	Path length (mean)	Invasion distance (mean)	Persistence (mean)	Single cell speed (mean)
Fiber length (mean)	n.s.	1.00**	0.9429*	n.s.
Fiber width (mean)	n.s.	0.9429*	1.00**	n.s.
Pore size (mean)	n.s.	0.8857*	0.9429*	n.s.

3.6.3 Fiber architecture drives long-term cell phenotype potentially by controlling initial cell shape

Next, we sought to investigate the matrix parameter(s) responsible for driving the collective cell phenotype observed P6-10 conditions. We observed that P6 appeared to be a transition point. We then identified matrix parameters that were exclusive to P6-10 conditions by using P4 as a cutoff. We found that only fiber length passed this criterion (Graphs 21-23). Interestingly, fiber length was also the only matrix parameter significantly correlated with cell shape. As a result, we hypothesized that fiber length could potentially be driving the observed phenotypic differences at the end of a week in culture, by controlling initial cell shape.

Graph 21. Fiber length potentially drives long-term cell phenotype. N=3 biological replicates for each condition. Statistical significance tested by ANOVA and reported as p<0.001, ***; p<0.01, **; p<0.05, *.

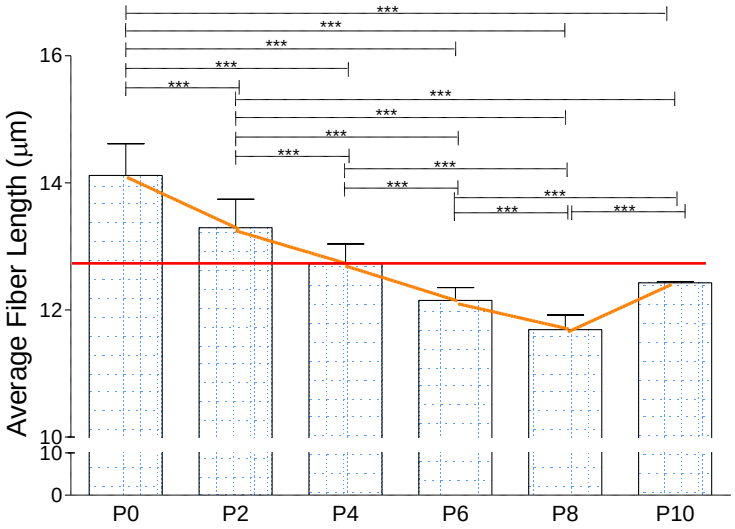

Graph 22. Fiber width potentially does not drive long-term cell phenotype. N=3 biological replicates for each condition. Statistical significance tested by ANOVA and reported as p<0.001, ***; p<0.01, **; p<0.05, *.

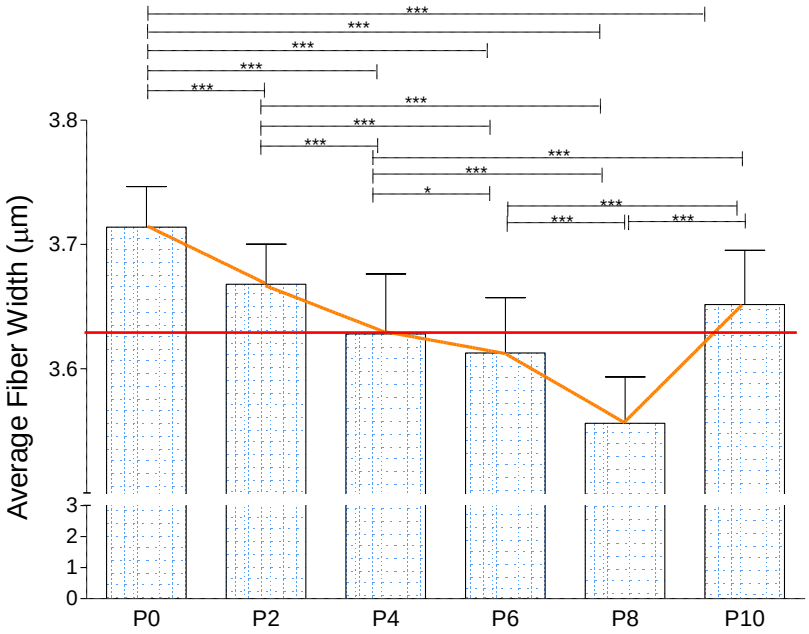

Graph 23. Pore size potentially does not drive long-term cell phenotype. N=3 biological replicates for each condition. Statistical significance tested by ANOVA and reported as p<0.001, ***; p<0.01, **; p<0.05, *.

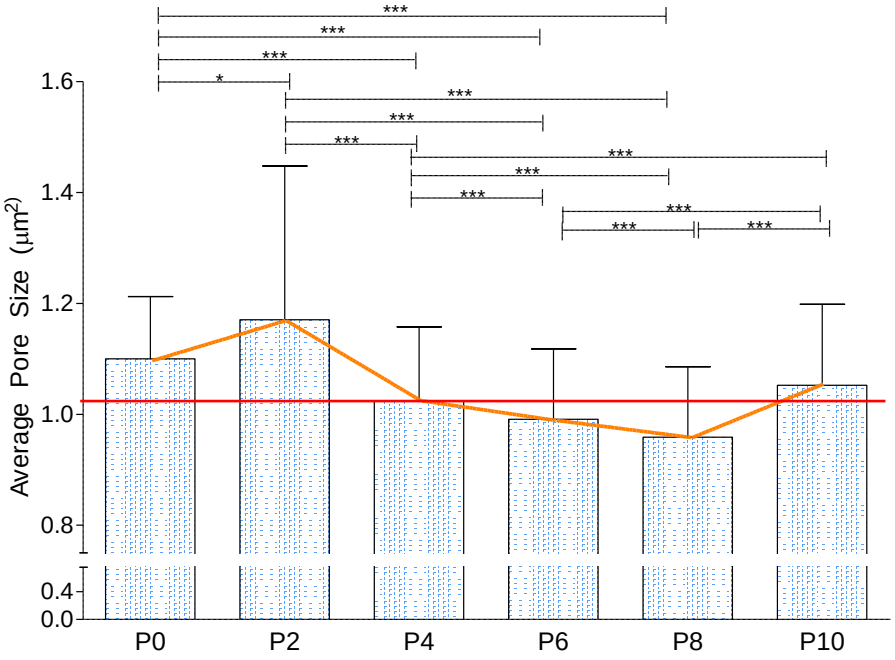

CHAPTER 4: DISCUSSION

Accumulating evidence suggests that matrix architecture is capable of modulating cell migration [12]–[14] as profoundly as matrix stiffness [15]–[17]. Largely, studies of matrix architecture have relied on micropatterned 2D surfaces and have focused on imparting contact guidance. Systematically controlling 3D ECM architecture remains a substantial challenge. Yet, it is now widely appreciated that the abundance, localization, and functional status of intracellular proteins can be significantly different in native 3D ECM culture compared to 2D models [18]–[20]. Thus, a major tradeoff exists between the physiological relevance of an ECM model system and the ability to tune and control specific features. It is currently impossible to decouple all of the architectural features of a 3D fibrillar protein network. Nonetheless, several studies have developed novel methods to produce highly aligned, anisotropic 3D collagen matrices, which impart both contact guidance and stiffness anisotropy [21]–[24]. These methods include magnetic, mechanical, and cell force driven reorganization of collagen fibers as well as electrospinning. Matrix stiffness and alignment modulate cell phenotype through mechanotransduction processes [25]. However, the mechanisms of action by which matrix architecture independently acts on cells is not clear. Here, we sought to create a novel 3D collagen system that retains physiological relevance while decoupling stiffness and density from fiber

architecture. Our study finds that collagen fiber topology independently mediates an MET-like phenotypic switch and implicates cell shape changes induced by matrix architecture as a potential mechanism. Furthermore, cell shape constraints and differences have been shown to regulate gene expression and transcription modules [26]. Future work will seek to elucidate the physicochemical processes involved.

While collagen is only one of many matrix components within the tissue and tumor microenvironment, both clinical and *in vivo* studies have established the relevance of this particular ECM molecule. Collagen is both an independent clinical prognostic indicator of cancer progression and a driver of tumorigenesis and metastasis. Thus, understanding how 3D collagen regulates cancer cell behavior is likely to provide useful insights into disease pathogenesis. A goal of future work in the field will be to explore in molecular detail the potential connections between 3D *in vitro* cancer phenotypes and clinical patient tumors rich in collagen.

The successful use of 8,000 Da PEG and 400,000 Da Ficoll [10] to tune matrix architecture with different structural outcomes suggests that other PEG chain sizes and functionalization could be explored with potentially different tuning effects. Likewise, the apparent saturation point we identified in our 10 mg/ml PEG condition, which began to reverse the trends in matrix parameters, could be extrapolated further as a potential means to segregate and bundle fibers.

CHAPTER 5: CONCLUSION AND FUTURE WORK

Interesting observations and correlations have been made in this work, but many new questions have arisen. Potential future work could entail experimentation with different sizes of PEG as the crowding agent. It would be interesting to determine whether a smaller PEG molecule could provide greater flexibility and matrix tunability. PEG can then also be used to tune other ECM hydrogels other than collagen I to assess the applicability of this MMC approach. Another potential direction is to investigate the *in vivo* implications and physiological relevance of the collective cell phenotype formed by breast cancer cells as a result of matrix architecture. This could potentially reveal a role for our 3D *in vitro* system as a model for studying cancer progression and aggressiveness. Ultimately, we have found potential relationships between certain matrix parameters and certain cellular responses and behaviors, but we do not currently understand the mechanistic basis for these associations. Further studies probing the physicochemical cues and pathways involved in the phenotypic switch we observe could help to reveal fundamental regulators of cell behavior. Similarly, it would be interesting to explore whether initial cell shape does indeed trigger different cell phenotypes to be adopted, potentially through transcriptional changes. Several of the matrix parameters we assessed reversed their response to PEG crowding in the P10 condition. We hypothesize that this could potentially be a sign of an artificially induced saturation effect or a limitation in the imaging modality that we used. A recent study has shown that CRM, while

widely used and accepted, is unable to image collagen fibers above approximately 50° from the imaging plane. While there is no reason to suspect a directional bias in the 3D matrices we polymerized, an alternative for imaging the collagen fibers would be confocal fluorescence microscopy (CFM), which was claimed to be able to detect nearly twice as many fibers than CRM could [27]. Even so, CRM is most likely sufficient for general characterization of various collagen matrices and for visualizing trends, but CFM is worth comparing to in order to obtain a more accurate and complete depiction. Finally, most of the matrix and cell analyses in this work were conducted within the first 24 hours of cell implantation. Cells behave very differently over time, perhaps switching on different transcriptional modules or varying the levels of MMP utilization. As such, studying embedded cells in more detail at later time points could reveal additional information. In summary, we believe that our novel collagen-PEG *in vitro* model serves as an important starting point and tool for studying cells in a tunable, and physiologically relevant and representative context, to elucidate phenomena that are conserved *in vivo*.

This thesis, in part, is currently being prepared for submission for publication of the material. Han, Anthony; Ortiz Velez, Daniel; Fraley, Stephanie I. The thesis author was the primary investigator and author of this material.

REFERENCES

[1] R. L. Siegel, K. D. Miller, and A. Jemal, “Cancer statistics,” *CA Cancer J Clin*, vol. 66, no. 1, pp. 7–30, 2016.

[2] P. Mehlen and A. Puisieux, “Metastasis: a question of life or death,” *Nat. Rev. Cancer*, vol. 6, no. 6, pp. 449–458, 2006.

[3] M. Sund and R. Kalluri, “Tumor stroma derived biomarkers in cancer,” *Cancer Metastasis Rev.*, vol. 28, no. 1–2, pp. 177–183, 2009.

[4] K. M. Riching *et al.*, “3D collagen alignment limits protrusions to enhance breast cancer cell persistence,” *Biophys. J.*, vol. 107, no. 11, pp. 2546–2558, 2015.

[5] J. L. Albritton and J. S. Miller, “3D bioprinting: improving *in vitro* models of metastasis with heterogeneous tumor microenvironments,” *Dis. Model. Mech.*, vol. 10, no. 1, pp. 3–14, 2017.

[6] V. Assi, J. Warwick, J. Cuzick, and S. W. Duffy, “Clinical and epidemiological issues in mammographic density,” *Nat. Rev. Clin. Oncol.*, vol. 9, no. 1, pp. 33–40, 2011.

[7] B. Weigelt, C. M. Ghajar, and M. J. Bissell, “The need for complex 3D culture models to unravel novel pathways and identify accurate biomarkers in breast cancer,” *Adv. Drug Deliv. Rev.*, vol. 69–70, pp. 42–51, 2014.

[8] S. I. Fraley, P. Wu, L. He, and Y. Feng, “Three-dimensional matrix fiber alignment modulates cell migration and MT1-MMP utility by spatially and temporally directing protrusions,” *Nat. Publ. Gr.*, no. October, pp. 1–13, 2015.

[9] B. N. Mason, A. Starchenko, R. M. Williams, L. J. Bonassar, and C. A. Reinhart-King, “Tuning three-dimensional collagen matrix stiffness independently of collagen concentration modulates endothelial cell behavior,” *Acta Biomater.*, vol. 9, no. 1, pp. 4635–4644, 2013.

[10] J. Dewavrin, N. Hamzavi, V. P. W. Shim, and M. Raghunath, “Acta Biomaterialia Tuning the architecture of three-dimensional collagen hydrogels by physiological macromolecular crowding,” *Acta Biomater.*, vol. 10, no. 10, pp. 4351–4359, 2014.

[11] P. R. O. Salvalaggio *et al.*, “Islet filtration: a simple and rapid new purification procedure that avoids ficoll and improves islet mass and function.,” *Transplantation*, vol. 74, no. 6, pp. 877–879, 2002.

[12] D. Ceballos, X. Navarro, N. Dubey, G. Wendelschafer-Crabb, W. R. Kennedy, and R. T. Tranquillo, “Magnetically Aligned Collagen Gel Filling a Collagen Nerve Guide Improves Peripheral Nerve Regeneration,” *Exp. Neurol.*, vol. 158, no. 2, pp. 290–300, 1999.

[13] N. Dubey, P. C. Letourneau, and R. T. Tranquillo, “Neuronal contact guidance in magnetically aligned fibrin gels: Effect of variation in gel mechano-structural properties,” *Biomaterials*, vol. 22, no. 10, pp. 1065–1075, 2001.

[14] A. L. Oliveira *et al.*, “Aligned silk-based 3-D architectures for contact guidance in tissue engineering,” *Acta Biomater.*, vol. 8, no. 4, pp. 1530–1542, 2012.

[15] M. J. Paszek *et al.*, “Tensional homeostasis and the malignant phenotype,” *Cancer Cell*, vol. 8, no. 3, pp. 241–254, 2005.

[16] G. Jiang, A. H. Huang, Y. Cai, M. Tanase, and M. P. Sheetz, “Rigidity Sensing at the Leading Edge through αvβ3 Integrins and RPTPα,” *Biophys. J.*, vol. 90, no. 5, pp. 1804–1809, 2006.

[17] C.-M. Lo, H.-B. Wang, M. Dembo, and Y. Wang, “Cell Movement Is Guided by the Rigidity of the Substrate,” *Biophys. J.*, vol. 79, no. 1, pp. 144–152, 2000.

[18] S. I. Fraley, Y. Feng, A. Giri, G. D. Longmore, and D. Wirtz, “Dimensional and temporal controls of three-dimensional cell migration by zyxin and binding partners,” *Nat. Commun.*, vol. 3, p. 719, 2012.

[19] S. I. Fraley *et al.*, “A distinctive role for focal adhesion proteins in three-dimensional cell motility,” *Nat. Cell Biol.*, vol. 12, no. 6, pp. 598–604, 2010.

[20] X. Yue, J. K. Lukowski, E. M. Weaver, S. B. Skube, and A. B. Hummon, “Quantitative Proteomic and Phosphoproteomic Comparison of 2D and 3D Colon Cancer Cell Culture Models,” *J. Proteome Res.*, vol. 15, no. 12, pp. 4265–4276, 2016.

[21] A. Ray, Z. M. Slama, R. K. Morford, S. A. Madden, and P. P. Provenzano, “Enhanced Directional Migration of Cancer Stem Cells in 3D Aligned Collagen Matrices,” *Biophys. J.*, vol. 112, no. 5, pp. 1023–1036, 2017.

[22] M. Antman-Passig, S. Levy, C. Gartenberg, H. Schori, and O. Shefi, “Mechanically Oriented 3D Collagen Hydrogel for Directing Neurite Growth,” *Tissue Eng. Part A*, vol. 23, p. ten.TEA.2016.0185, 2017.

[23] P. P. Provenzano, K. W. Eliceiri, D. R. Inman, and P. J. Keely, “Engineering three-dimensional collagen matrices to provide contact guidance during 3D cell migration,” *Curr. Protoc. Cell Biol.*, no. SUPPL. 47, pp. 1–11, 2010.

[24] Y. L. Chang *et al.*, “Correlation Between Serum Prostate Specific Antigen and Prostate Volume in Taiwanese Men With Biopsy Proven Benign Prostatic Hyperplasia,” *J. Urol.*, vol. 176, no. 1, pp. 196–199, 2006.

[25] A. J. Engler, M. A. Griffin, S. Sen, C. G. Bönnemann, H. L. Sweeney, and D. E. Discher, “Myotubes differentiate optimally on substrates with tissue-like stiffness: Pathological implications for soft or stiff microenvironments,” *J. Cell Biol.*, vol. 166, no. 6, pp. 877–887, 2004.

[26] N. Jain, K. V. Iyer, A. Kumar, and G. V. Shivashankar, “Cell geometric constraints induce modular gene-expression patterns via redistribution of HDAC3 regulated by actomyosin contractility,” *Proc. Natl. Acad. Sci.*, vol. 110, no. 28, pp. 11349–11354, 2013.

[27] D. A. Vader, B. Fabry, D. A. Weitz, L. M. Jawerth, and S. Mu, “A Blind Spot in Confocal Reflection Microscopy : The Dependence of Fiber Brightness on Fiber Orientation in Imaging Biopolymer Networks,” vol. 98, no. February 2009, pp. 3–5, 2010.